Terahertz surface plasmon polaritons on a semiconductor surface structured with periodic V-grooves

Shanshan Li,[1] Mohammad M. Jadidi,[1] Thomas E. Murphy[1,2] and Gagan Kumar[2,*]

[1]*Department of Electrical & Computer Engineering University of Maryland, College Park, MD 20742, USA*

[2]*Institute for Research in Electronics & Applied Physics University of Maryland, College Park, MD 20742, USA*

[*]*gkm2010@umd.edu*

Abstract: We demonstrate propagation of terahertz waves confined to a semiconductor surface that is periodically corrugated with V-shaped grooves. A one-dimensional array of V-grooves is fabricated on a highly-doped silicon surface, using anisotropic wet-etching of crystalline silicon, thereby forming a plasmonic waveguide. Terahertz time domain spectroscopy is used to characterize the propagation of waves near the corrugated surface. We observe that the grating structure creates resonant modes that are confined near the surface. The degree of confinement and frequency of the resonant mode is found to be related to the pitch and depth of the V-grooves. The surface modes are confirmed through both numerical simulations and experimental measurements. Not only does the V-groove geometry represent a new and largely unexplored structure for supporting surface waves, but it also enables the practical fabrication of terahertz waveguides directly on semiconductor surfaces, without relying on reactive-ion etching or electroplating of sub-millimeter metallic surfaces.

OCIS codes: (240.6680) Surface plasmons; (240.6690) Surface waves; (230.4555) Coupled resonantors.

References and links

1. H. Raether, *Surface plasmons on smooth and rough surfaces and on grattings*, vol. 111 of *Springer tracts in modern physics* (Springer, 1988).
2. T.-I. Jeon and D. Grischkowsky, "THz Zenneck surface wave (THz surface plasmon) propagation on a metal sheet," Appl. Phys. Lett. **88**, 061113 (2006).
3. P. Berini, "Long-range surface plasmon polaritons," Adv. Opt. Photon. **1**, 484–588 (2009).
4. K. Wang and D. M. Mittleman, "Metal wires for terahertz wave guiding," Nature **432**, 376–379 (2004).
5. S. A. Maier and S. R. Andrews, "Terahertz pulse propagation using Plasmon-polariton-like surface modes on structures conductive surface," Appl. Phys. Lett. **88**, 251120 (2006).
6. G. Kumar and V. K. Tripathi, "Surface enhanced Raman Scattering of a surface plasma wave," J. Phys. D: Appl. Phys. **39**, 4436–4439 (2006).
7. Z. Tian, R. Singh, J. Han, J. Gu, Q. Xing, J. Wu, and W. Zhang, "Terahertz superconducting plasmonic hole array," Opt. Lett. **35**, 3586–3588 (2010).
8. J. N. Anker, W. P. Hall, O. Lyandres, N. C. Shah, J. Zhao, and R. P. Van Duyne, "Biosensing with plasmonic nanosensors," Nature Mater. **7**, 442–453 (2008).
9. S. Palomba, M. Danckwerts, and L. Novotny, "Nonlinear plasmonics with gold nanoparticle antennas," J. Opt. A: Pure Appl. Opt. **11**, 114030 (2009).

#179340 - $15.00 USD Received 9 Nov 2012; revised 27 Jan 2013; accepted 28 Feb 2013; published 13 Mar 2013

10. P. L. Stiles, J. A. Dieringer, N. C. Shah, and R. P. Van Duyne, "Surface-enhanced Raman spectroscopy," Annu. Rev. Anal. Chem. **1**, 601–26 (2008).
11. A. V. Zayats, I. I. Smolyaninov, and A. A. Maradudin, "Nano-optics of surface plasmon polaritons," Phys. Reports **408**, 131–314 (2005).
12. J. B. Pendry, L. Martín-Moreno, and F. J. García-Vidal, "Mimicking surface plasmons with structured surfaces," Science **305**, 847–848 (2004).
13. Z. Ruan and M. Qiu, "Slow electromagnetic wave guided in subwavelength region along one-dimensional periodically structured metal surface," Appl. Phys. Lett. **90**, 201906 (2007).
14. W. Zhu, A. Agrawal, A. Cui, G. Kumar, and A. Nahata, "Engineering the propagation properties of planar plasmonic terahertz waveguides," IEEE J. of Select. Topics Quant. Electron. **17**, 146–153 (2011).
15. C. R. Williams, S. R. Andrews, S. A. Maier, A. I. Fernández-Domínguez, L. Martín-Moreno, and F. J. García-Vidal, "Highly confined guiding of terahertz surface plasmon polaritons on structured metal surfaces," Nature Photon. **2**, 175–179 (2008).
16. F. J. Garcia-Vidal, L. Martín-Moreno, and J. B. Pendry, "Surfaces with holes in them: new plasmonic metamaterials," J. Opt. A: Pure Appl. Opt. **7**, S97–S101 (2005).
17. G. Kumar, S. Pandey, A. Cui, and A. Nahata, "Planar plasmonic terahertz waveguides based on periodically corrugated metal films," New J. Phys. **13**, 033024 (2011).
18. J. G. Rivas, M. Kuttge, P. H. Bolivar, and H. Kurz, "Propagation of surface plasmon polaritons on semiconductor gratings," Phys. Rev. Lett. **93**, 256804 (2004).
19. W. Zhao, O. M. Eldaiki, R. Yang, and Z. Lu, "Deep subwavelength waveguiding and focusing based on designer surface plasmons," Opt. Express **18**, 21498–21503 (2010).
20. T. Jiang, L. Shen, J.-J. Wu, T.-J. Yang, Z. Ruan, and L. Ran, "Realization of tightly confined channel plasmon polaritons at low frequencies," Appl. Phys. Lett. **99**, 261103 (2011).
21. A. I. Fernández-Domínguez, E. Moreno, L. Martín-Moreno, and F. J. Garcia-Vidal, "Terahertz wedge plasmon polaritons," Opt. Lett. **34**, 2063–2065 (2009).
22. S. I. Bozhevolnyi and J. Jung, "Scaling for gap plasmon based waveguides," Opt. Express **16**, 2676–2684 (2008).
23. F. Liu, S. Peng, H. Jia, M. Ke, and Z. Liu, "Strongly localized acoustic surface waves propagating along a V-groove," Appl. Phys. Lett. **94**, 023505–3 (2009).
24. Y. J. Zhou, Q. Jiang, and T. J. Cui, "Bidirectional bending splitter of designer surface plasmons," Appl. Phys. Lett. **99**, 111904 (2011).
25. C. L. C. Smith, B. Desiatov, I. Goykmann, I. Fernandez-Cuesta, U. Levy, and A. Kristensen, "Plasmonic V-groove waveguides with Bragg grating filters via nanoimprint lithography," Opt. Express **20**, 5696–5706 (2012).
26. S. I. Bozhevolnyi, V. S. Volkov, E. Devaux, and T. W. Ebbesen, "Channel plasmon-polariton guiding by subwavelength metal grooves," Phys. Rev. Lett. **95**, 046802 (2005).
27. S. I. Bozhevolnyi, V. S. Volkov, E. Devaux, J.-Y. Laluet, and T. Ebbesen, "Channel plasmon subwavelength waveguide components including interferometers and ring resonators," Nature **440**, 508–511 (2006).
28. J. J. Wood, L. A. Tomlinson, O. Hess, S. A. Maier, and A. I. Fernández-Domínguez, "Spoof plasmon polaritons in slanted geometries," Phys. Rev. B **85**, 075441 (2012).
29. S. Sriram and E. P. Supertzi, "Novel V-groove structures on silicon," Appl. Opt. **24**, 1784–1787 (1985).
30. U. Fano, "Effects of configuration interaction on intensities amd phase shifts," Phys. Rev. **124**, 1866–1878 (1961).
31. A. Agrawal, T. Matsui, Z. V. Vardeny, and A. Nahata, "Terahertz transmission properties of quaisperiodic and aperiodic aperature arrays," J. Opt. Soc. Am. B **24**, 2545–2555 (2007).

1. Introduction

In recent years, electromagnetic waves propagating at the interface between a metal and dielectric have been of significant interest [1–7]. These waves allow for sub-wavelength confinement of the field, overcoming the diffraction limit, and opening the possibility for unprecedented device miniaturization. Possible applications of surface waves include bio-sensing [8], nonlinear phenomenon [9], material characterization and surface enhanced Raman scattering [6, 10].

At visible and near infrared frequencies, many conventional metal surfaces support localized surface plasmon polariton modes that can be excited using prism-coupling methods [11]. Such methods cannot be applied at terahertz frequencies, where most metals behave more like perfect electrical conductors. In 2004, Pendry et. al proposed the introduction of a periodic texture to a conducting surface in order to compensate for the wavevector mismatch, thus allowing for excitation of surface waves with a wavenumber that exceeds that of the excitation [12]. Thereafter, extensive experimental and theoretical work has been reported on the excitation and confinement of surface waves using surface corrugations [13–19]. Highly confined surface

#179340 - $15.00 USD Received 9 Nov 2012; revised 27 Jan 2013; accepted 28 Feb 2013; published 13 Mar 2013

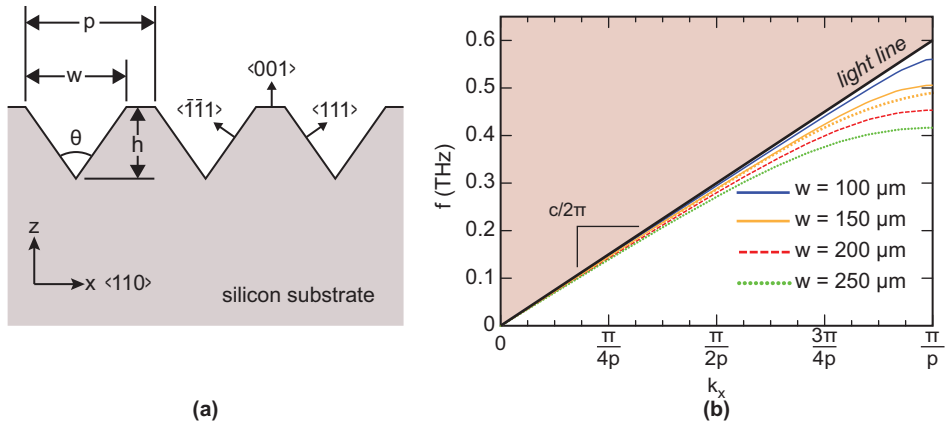

Fig. 1. (a) Geometry of semiconductor plasmonic V-groove waveguide fabricated on a silicon substrate. The width and height are related by $w/h = 2\tan(\theta/2) = \sqrt{2}$. (b) Numerically computed dispersion relations of the fundamental surface mode for three different line widths (w).

modes have been demonstrated in several geometries, including metallic apertures, blind holes, rectangular gratings, and others. Most of these devices have used laser micromachining, or planar photolithographic techniques such as liftoff, reactive-ion etching, thin-film deposition, and electroplating to form rectangular conductive features on a substrate.

More recently, other geometries have been proposed for plasmonic waveguides, including triangular surface grooves [20–25]. At telecommunication wavelengths, isolated V-groove structures have been experimentally verified to guide channel plasmon polariton with subwavelength confinement and low loss at bends [26, 27]. More recently, Wood *et al.* numerically analyzed a surface plasmon mode sustained by periodic array of slanted rectangular grooves in a conductive substrate [28]. Fabrication of non-rectangular grooves in a metallic substrate has proved challenging because of the difficulty of patterning or etching metal, and consequently most of the prior research on such structures has been numerical.

In crystalline silicon, V-groove geometries can be readily fabricated by employing anisotropic wet etching [29]. At terahetz frequencies, silicon can exhibit metallic properties when heavily doped and can be used to efficiently propagate spoof plasmon polaritons when patterned with subwavelength structures. Unlike metals, the dielectric properties of silicon can be adjusted by controlling the dopant concentration which in turn determines the degree of confinement and the loss for the plasmonic wave – an additional degree of freedom that is unavailable in most plasmonic substrates.

In this paper, we report terahertz spoof plasmon polariton propagation on a highly doped silicon surface that is patterned with periodic V-grooves. Terahertz time domain spectroscopy is used to characterize the surface wave, and shows evidence of a resonant mode that is confined to the surface. Numerical and experimental measurements reveal that the resonant frequency and degree of confinement can be adjusted by tailoring the depth and period of the V-grooves. Numerical simulations reveal that deeper V-grooves can provide tighter surface confinement and slower group velocities for the resonant mode. In section 2 of the paper, we discuss the dispersion properties of the surface modes supported by the proposed geometry. In section 3, we describe the experimental setup and device fabrication. The experimental and numerically simulated measurements are presented in section 4, and the results are summarized in section 5.

#179340 - $15.00 USD Received 9 Nov 2012; revised 27 Jan 2013; accepted 28 Feb 2013; published 13 Mar 2013

2. Numerical analysis of the surface modes

Figure 1(a) depicts the geometry of the semiconductor plasmonic waveguide considered here. The substrate is comprised of crystalline silicon that is patterned through anisotropic etching, such that the sides of the V-grooves are parallel to the $\langle 111 \rangle$ and $\langle \overline{111} \rangle$ crystallographic planes. The apex angle θ is therefore constrained to be $\theta = \tan^{-1}\sqrt{8} = 70.53^{\circ}$, and the width to height ratio is likewise constrained to be $w/h = 2\tan(\theta/2) = \sqrt{2}$. The pitch and height of the corrugation can be controlled through lithographic processing.

Figure 1(b) depicts the calculated dispersion relation for three different grating line widths of w = 100, 150, 200, and 250 μm, each with the same grating pitch of p = 250 μm. The dispersion curves were calculated using the finite element method, and the solid black curve indicates the light line for wave propagation in the free-space region.We used a hexahedral mesh in simulation with a grid size of one-tenth of the period. Perfectly matched boundary layers were used at the edges of the computational domain, and the conductivity in simulations was based upon the resistivity of the highly doped silicon used in experiment.We note that as the width (and hence the depth) of the V-grooves is increased, the dispersion of the wave shows a pronounced curvature away from the light line, indicating slower phase and group velocities, especially near the first Brillouin edge. In order to study the effect of dopant concentration on the surface mode behaviour, we numerically simulated the grating structures of width w = 100 with two different dopant concentrations. The orange curves in solid and dotted lines correspond to the dopant concentration of 4×10^{20} cm^{-3} and 5×10^{18} cm^{-3}, respectively. One may note that as the dopant concentration decreases, the dispersion curve gets red-shifted due to increase in the effective penetration depth of the terahertz in V-grooves. At the same time waveguide loss is expected to increase.

3. Experimental details and fabrication of samples

The devices described here were fabricated starting from $\langle 100 \rangle$ boron-doped p-type silicon wafers with a resistivity of 2-5 mΩ cm (dopant concentration, $n \sim 4 \times 10^{20}$ cm^{-3}). This dopant concentration corresponds to a plasma frequency of 290 THz. A silicon dioxide layer of thickness 1.2 μm was deposited on the silicon substrate using low pressure chemical vapor deposition (LPCVD). This layer was then patterned using contact photolithography followed by wet etching in buffered hydrofluoric acid, to produce a periodic array of openings in the SiO_2 film. The sample was then immersed in a solution of potassium hydroxide, water, and isopropanol in the ratio of 60:30:10 at a temperature of 80° C to perform the anisotropic etching which forms the V-grooves. During the etching, the depth of the V-groove h was estimated to increase at approximately 0.4 μm/s. Following the etching, the remaining oxide mask layer was removed in a buffered hydrofluoric acid solution. Figure 2(a) shows a representative cross-sectional scanning electron micrograph of a completed structure. The grating lines were each 30 mm wide, which was much larger than the terahertz beam size, thus ensuring that the propagation could be adequately approximated as a two-dimensional structure. Each waveguide was composed of an array containing 200 grating lines at a pitch of p = 250 μm, for a total length of 50 mm. Groove widths of w = 100 μm and 200 μm were fabricated (with corresponding depths of 71 and 141 μm). It should be noted that comparing with the wavelength of interest discussed below, the considered parameters indicate that we are operating in the subwavelength limit.

In order to facilitate coupling from a free-space terahertz beam into the plasmonic waveguide, a second photolithographic step was used to pattern a shallow 300 μm wide groove at 5 mm away from the edge of the V-groove array. This groove was etched to a depth of 100 μm using deep reactive ion etching (Bosch process.) When a terahertz beam from free space impinges at normal incidence onto the coupling groove, a portion of the radiation scatters into the plasmonic

#179340 - $15.00 USD Received 9 Nov 2012; revised 27 Jan 2013; accepted 28 Feb 2013; published 13 Mar 2013

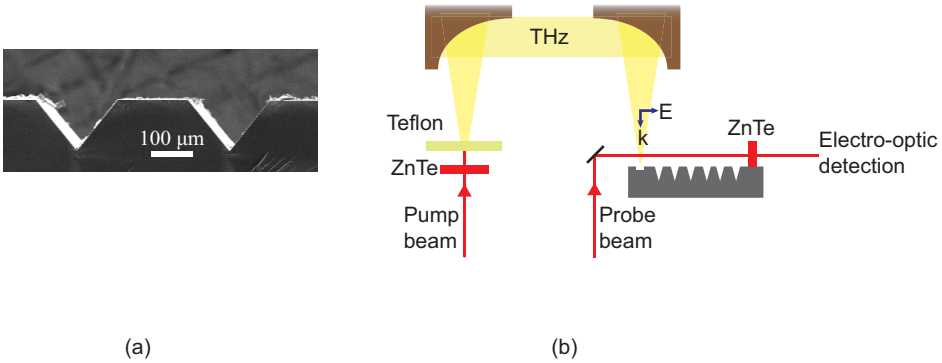

Fig. 2. (a) The SEM image of a portion of the fabricated structure (side view). (b) Schematic of the experimental setup. The ZnTe crystal is used to generate terahertz via photo-rectification. The detection is done via electro-optic sampling using 1 mm thick (110) ZnTe crystal.

waveguide mode.

Figure 2(b) depicts the terahertz time-domain spectroscopy system used to characterize the plasmonic waveguides. Pulses from an amplified Ti:sapphire laser system were split (80:20) into pump and probe beams that generate and detect the terahertz waveforms, respectively. The optical pulses were 43 fs in duration, at a repetition period of 1 kHz and a central wavelength of 800 nm. Terahertz pulses were generated using optical rectification in a 1 mm thick $\langle 110 \rangle$-oriented ZnTe crystal, with an input pulse energy of 1.2 mJ and beam diameter of 10 mm. The pump beam was synchronously chopped at a rate of 250 Hz. The terahertz radiation was collected and collimated using off-axis parabolic mirrors, and focused at normal incidence onto the rectangular coupling groove. The impinging terahertz beam was linearly polarized in the direction perpendicular to the grooves (i.e., with the magnetic field parallel to the grooves), in order to ensure that the scattered radiation couples into the TM-polarized plasmonic mode of the structure.

At the opposite edge of the corrugated structure, the emerging terahertz beam was electrooptically sampled using a similar ZnTe crystal of size 3 x 3 mm, which was brought into contact with the substrate. The probe beam of diameter less than 0.5 mm was adjusted to co-propagate with the terahertz wave through the ZnTe crystal at a height of 0.5 mm from the surface. Following the electrooptic crystal, a quarter wave plate, Wollaston prism, balanced photoreceiver, transimpedance amplifier, and lock-in detector (not shown) were used to measure the terahertz electric field as the delay τ between the pump and probe was swept using a motorized translation stage.

4. Results and discussions

Figure 3 shows the experimentally observed transmitted terahertz waveforms, together with numerical simulations obtained using a finite element method based time-domain simulation. Figure 3(a) depicts the input terahertz waveform, measured by redirecting the terahertz wave directly to the electrooptic detector with the silicon waveguide absent.

Figure 3(b) shows the terahertz spectrum measured at the output of the V-groove array, for the case when the grating line width was w = 100 μm. The blue curve shows the calculated spectrum obtained by numerically simulating the structure using the input waveform taken in Fig. 3(a). Both the theory and numerical simulation show a pronounced null in the transmitted spectrum at a frequency of 0.58 THz. This frequency matches the frequency at the first Bril-

#179340 - $15.00 USD Received 9 Nov 2012; revised 27 Jan 2013; accepted 28 Feb 2013; published 13 Mar 2013

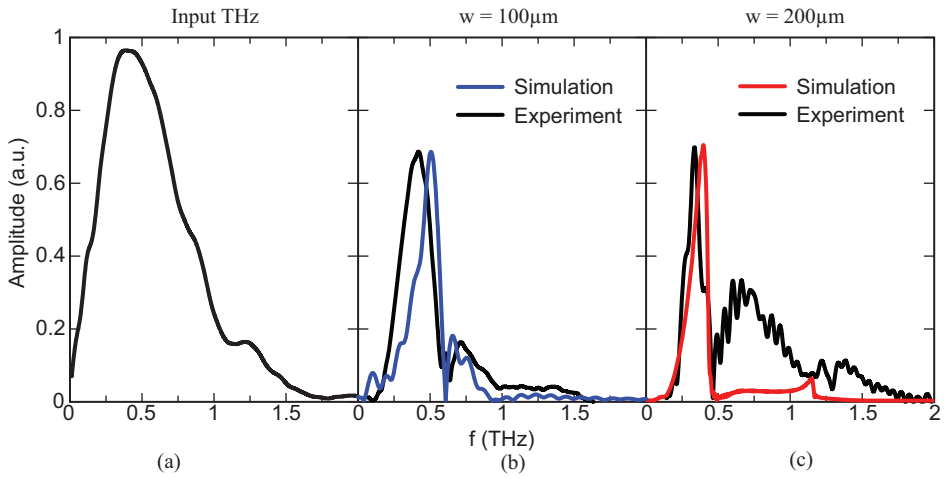

Fig. 3. Experimentally measured frequency domain transmission spectra: (a) THz input signal used in the experiments, measured in back-to-back configuration. (b) Simulated (blue) and measured (black) transmission spectrum for plasmonic V-groove waveguide with w = 100 μm. (c) Simulated (red) and measured (black) transmission spectrum for plasmonic V-groove waveguide with w = 200 μm.

louin edge in Fig. 1, where the wavevector reaches p/π. The occurrence of null in the spectrum can be attributed to the interference effect occurring between the discrete resonance caused by the diffraction from the corrugations and the continuum transmission spectrum on the surface associated with the waveguide geometry. The interference effect between discrete and broad spectrum has been studied in the literature [30, 31]. The terahertz wave at the resonance associated with the null get strongly trapped to the grating leading to the strong confinement. The experimental measurements show weak Fabry-Pérot spectral fringes associated with multiple internal reflections inside of the ZnTe detection crystal, an effect that is not modeled in the simulation.

Figure 3(c) shows similar results obtained when w = 200 μm. In this case, the frequency at null associated with the fundamental resonance shifts to 0.46 THz, again in agreement with the frequency at the first Brillouin edge in Fig. 1. The measurements and simulations further reveal a higher-order resonance at approximately 1.2 THz.

The disagreement between the experimental observations and numerical simulations in the higher frequency range is thought to be caused by numerical inaccuracies in the simulation that become more pronounced at short wavelengths. In particular, while a mesh size of $p/10$ may be sufficient to accurately predict the performance at long wavelengths, we anticipate greater quantization errors at frequencies above the first Brillouin boundary. Moreover, rather than simulate the plasmonic excitation and terahertz detection scheme used in the experiment, we employed a more numerically tractable approach of introducing and detecting the signal through a finite-sized excitation ports at the edges of the computational window. As a result, our numerical simulations may not be as sensitive to the effects of scattered signals as the experiment. Further, we note that the effect of scattering is expected to be stronger for the deep grating shown in Fig. 3(c) than for the shallow grating of Fig. 3(b). We note that earlier papers have reported in similar discrepancies in the higher frequency regime [17].

To better illustrate the nature of the resonant plasmonic confinement, in Fig. 4 (Media 1–4) we plot the electric field profiles for the case when w = 200 μm, calculated at four different

#179340 - $15.00 USD Received 9 Nov 2012; revised 27 Jan 2013; accepted 28 Feb 2013; published 13 Mar 2013

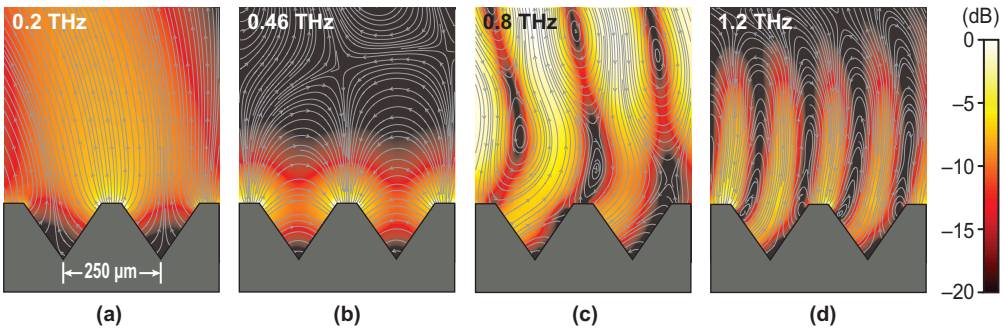

Fig. 4. Electric fields calculated for w = 200 μm at four different frequencies below and above the resonant frequency: (a) 0.2 THz, below resonance (Media 1), (b) 0.46 THz, on resonance (Media 2), (c), 0.8 THz, above resonance (Media 3), and (d) 1.2 THz, second-order resonance (Media 4). The static frames shown here were captured at the peak of each cycle.

frequencies. The online supplemental media files contain an animated view of the field evolution, which more clearly distinguishes the standing wave and travelling wave characteristics of the fields. The static frames presented in Fig. 4 were captured at times during an optical cycle when the fields achieve their maximum strength.

Figure 4(a) (Media 1) shows the electromagnetic fields calculated at 0.2 THz, which is below the plasmonic resonant frequency. In this case, the wave propagation resembles as an unbound travelling wave above the surface, with no significant confinement in the periodic structure. In contrast, Fig. 4(b) (Media 2) shows the fields computed at the resonant frequency of 0.46 THz. On resonance, the electromagnetic fields remain confined near the surface and inside of the V-grooves, and the spatial periodicity of the wave matches that of the grating. The animation (Media 1) further illustrates the hybrid standing-wave / travelling-wave character of the resonant solution, which is expected for slow-wave structures. Figure 4(c) shows the calculated fields at 0.8 THz (above resonance), again showing no significant surface confinement. Finally, in Fig. 4(d) we show the field profile at a frequency of 1.2 THz, which corresponds to a second-order resonance. In this case, the spatial periodicity of the wave matches the second spatial harmonic of the grating corrugation, and we again see plasmonic confinement near the surface (albeit a weaker confinement than for the fundamental resonance.)

The degree of confinement in the plasmonic structure is closely correlated with the depth of the V-grooves, with deeper features producing stronger confinement. The relationship is explicitly discussed toward the end of this paper. However, because of the anisotropic etching process used to fabricate the structures, the grating depth is restricted to be equal to $w/\sqrt{2}$. We note, however, that alternative fabrication methods, such as reactive ion etching, could potentially be used to produce V-grooves with much higher aspect ratios. Next we numerically analyze deeper V-grooves with a fixed width. Figure 5(a) plots the calculated dispersion relation for four different plasmonic waveguides for which the pitch and width are fixed at p = 250 μm and w = 150 μm, respectively, but the apex angle is decreased from $\theta = 90^\circ$ to 20°. As before, in all cases the grating exhibits a resonant frequency at the edge of the Brillouin zone boundary, at which point the surface wave was found to be localized near the conductive surface. The steeper apex angles produce a much stronger deviation from the light line and a tighter confinement in the groove. Figure 5(b) shows the related group velocity, obtained after numerically finding the slope of the dispersion curve. The steeper (and hence deeper) gratings show a slower group velocity, associated with tighter confinement in the V-grooves.

#179340 - $15.00 USD Received 9 Nov 2012; revised 27 Jan 2013; accepted 28 Feb 2013; published 13 Mar 2013

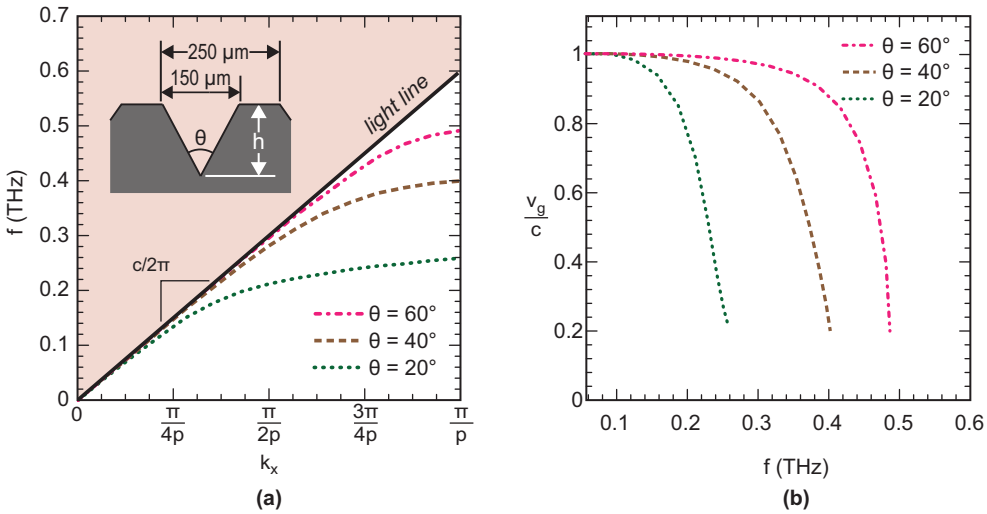

Fig. 5. (a) Numerically calculated dispersion relation for the surface modes supported by a conductive grating structure with $p = 250\ \mu$m, $w = 150\mu$m, and $\theta = 90^\circ, 60^\circ, 40^\circ, 20^\circ$. (b) The associated group velocity dispersion for the three structures considered in (a), showing the progressively slower wave velocities attained by increasing the depth of the grooves.

In order to explain the correlations between the depth of the V-groove, the confinement of the surface mode, and the reduction in group velocity, we consider the special case of V-groove with an apex angle of 90°, which can be generalized from the recent analysis of Wood et al. [28]. In this case, the dispersion relation using quasi-analytical approach in the long wavelength limit and neglecting the higher order diffraction terms may be written as

$$k_x = k_0 \left[1 + 2 \left(\frac{h}{p} \tan \left(\frac{k_0 h}{\sqrt{2}} \right) \mathrm{sinc}^{-1} \left(\frac{k_0 h}{\sqrt{2}} \right) \right)^2 \right]^{1/2} \tag{1}$$

where k_x is the propagation constant in the x-direction (traveling wave direction), k_0 is the free space propagation constant, h is the depth of the groove from the apex to the surface in normal direction and p is the periodicity. For the traveling surface plasma wave which has major component of the electric field in the transverse and the propagation direction, the transverse confinement factor (α) can be calculated as

$$\alpha = \left(k_x^2 - k_0^2 \right)^{1/2} \tag{2}$$

From the dispersion relation given in Eq. (1), one may easily calculate the group velocity of the traveling surface wave. We plot in Fig. 6 the confinement factor α and group velocity of the surface bound wave as a function of frequency for two different depths of h = 50 μm and h = 75 μm, using $p = 250\ \mu$m and $\theta = 90^\circ$. One may note that confinement factor increases with the frequency while group velocity decreases. At any frequency considered, the deeper grooves show a higher confinement factor and smaller group velocity than the corresponding shallow-groove structure. Although the theoretical relationship only applies to the special case of $\theta = 90^\circ$, our numerical simulations suggest that these general relations should also hold true for other V-groove structures as well.

#179340 - $15.00 USD Received 9 Nov 2012; revised 27 Jan 2013; accepted 28 Feb 2013; published 13 Mar 2013

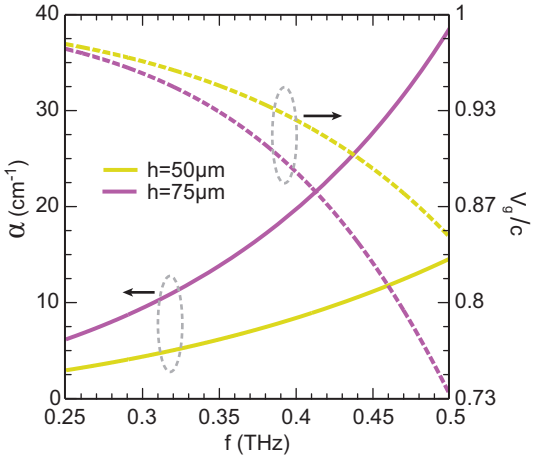

Fig. 6. Variation of confinement factor and group velocity of the fundamental surface mode with the terahertz frequency for two different depths i.e. $h = 50$ μm and $h = 75$ μm of V-grooves. The solid line corresponds to confinement while the dotted curves corresponds to the group velocity of the surface mode.

5. Conclusions

We described the analysis, theory, fabrication, and measurement of a semiconductor plasmonic THz waveguide that uses a p^+-doped silicon as the conductive substrate that is patterned into an array of V-grooves through anisotropic wet chemical etching. The structures are simulated using finite element methods, and measured using a terahertz time-domain spectroscopy system that was modified to sample surface fields. Measurements and simulations both show evidence of a resonant surface wave that occurs when $k_x = \pi/p$, with a reduced group velocity. The field confinement, the degree of reduction in group velocity, and the resonant frequency are related to the corrugation shape, with deeper structure producing a more pronounced effect. The study could play an important role in the developments of active and passive semiconductor devices operating at terahertz frequencies.

Acknowledgments

This work was sponsored by the Office of Naval Research, through the University of Maryland Center for Applied Electromagnetics (Grant No. N000140911190) with the support of the Maryland NanoCenter and its NispLab and FabLab.

#179340 - $15.00 USD Received 9 Nov 2012; revised 27 Jan 2013; accepted 28 Feb 2013; published 13 Mar 2013